



## Reversible martensite transformations in thermal cycled polycrystalline Cu-13.7%Al-4.0%Ni alloy



Elaine C. Pereira<sup>a</sup>, Lioudmila A. Matlakhova<sup>a,\*</sup>, Anatoly N. Matlakhov<sup>a,1</sup>, Carlos J. de Araújo<sup>b</sup>, Carlos Y. Shigue<sup>c</sup>, Sergio N. Monteiro<sup>d</sup>

<sup>a</sup> Laboratory for Advanced Materials (LAMAV), State University of the Northern of Rio de Janeiro, Advanced Materials Laboratory, Brazil

<sup>b</sup> Federal University of Campina Grande, Dept. of Mechanical Engineering, Brazil

<sup>c</sup> School of Engineering Lorena (EEL-USP) of the University of São Paulo (USP), College of Engineering, Brazil

<sup>d</sup> Military Institute of Engineering of the Rio de Janeiro (IME-RJ), Brazil

### ARTICLE INFO

#### Article history:

Received 22 March 2016

Received in revised form

18 July 2016

Accepted 19 July 2016

Available online 22 July 2016

#### Keywords:

Cu-Al-Ni alloy

Polycrystalline structure

Martensitic transformation

Thermal cycling treatment

Microhardness

### ABSTRACT

A polycrystalline copper alloy with 13.7 wt% aluminum and 4.0 wt% nickel, produced by plasma fusion followed by injection molding, was investigated for the reversible martensitic transformations (RMT) occurring in association with load-free thermal cycling treatments (TCT's). The as-received quenched alloy was subjected to distinct TCT's up to 500 cycles within the temperature interval from 258 K (below  $M_f$ ) to 373 K (above  $A_f$ ). Each distinct TCT was finished at room temperature (RT) either by half cooling cycle (258 K to RT) or by half heating cycle (373 K to RT). Transformations were characterized by X-ray diffraction, differential scanning calorimetry, optical microscopy and microhardness. The results revealed a complex sequence of transformations involving the high temperature  $\beta_1$  phase, the metastable  $\gamma_1'$  and  $\beta_1'$  martensitic phases, and the intermediate  $Al_7Cu_4Ni$  phase, known as the R phase. Depending on the number of cycles and the finishing way, the sequence of transformations was partial or complete. The RMT with TCT promotes different changes in the microstructure, including an apparent pull out of grains. Microhardness was also sensibly affected owing to the complex participation of different phases.

© 2016 Elsevier B.V. All rights reserved.

### 1. Introduction

Cu-Al-Ni alloys based on the intermetallic compound  $Cu_3Al$  may undergo reversible martensitic transformations (RMT) involving the reaction  $\beta_1 \leftrightarrow \beta_1' + \gamma_1'$  by either thermal-only or load-assisted treatments [1–4]. These RMT-prone alloys, known as shape memory alloys (SMA) due to the associated effect, are currently gaining attention owing to special advantages, over the more commonly used Ti-Ni, Cu-Zn and Cu-Zn-Al alloys, for industrial applications using actuator devices. Superior thermal and electrical conductivities as well as lower cost have been reported [5–7].

In order to perform memory effect under repetitive condition, which is required by an actuator device, SMA requires multiple heating and cooling cycles within an interval, usually between

173 K and 573 K, covering the critical RMT temperatures. During typical operations, a SMA may suffer an extensive number of thermal cycles. In this regard, RMT-prone Cu-Al-Ni alloys are expected to display a comparatively better performance, particularly as single crystals [8].

It is well known that a thermal cyclic treatment (TCT) may promote not only modifications in the alloy structure and composition but also changes in its physical and mechanical properties [9,10]. Single crystals of RMT-prone Cu-Al-Ni alloys endure TCT in an efficient way, associated with an improvement in its life to fracture [7,11]. Inhibition of the  $\gamma_1'$  martensite formation was found in these single crystal alloys as the number of cycles increases [12–15]. In particular, Araujo et al. [15] detected an increase of the critical transformation temperature in association with a change of  $\gamma_1'$  into  $\beta_1'$  after a long enough aging time at 473 K.

By contrast to single crystals, polycrystalline Cu-Al-Ni alloys, in spite of displaying shape memory effect with superior conductivities, have traditionally been unconsidered for practical applications due to their brittle behavior associated with intergranular fracture. This might occur even after a reduced number of either

\* Corresponding author. Advanced Materials Laboratory, State University of the Northern Rio de Janeiro, Avenida Alberto Lamego, 2000, Parque California, Campos dos Goytacazes, CEP 28013-602, RJ, Brazil.

E-mail address: [lioudmila@uenf.br](mailto:lioudmila@uenf.br) (L.A. Matlakhova).

<sup>1</sup> He died in 15.10.2011.

thermal-only, mechanical (load-assisted) or thermo-mechanical cycles is imposed. Sakamoto and Shimizu [16,17] indicated four possible reasons for a SME polycrystal intergranular fracture: (a) incompatibility of elastic deformation due to a high anisotropy; (b) incompatibility of deformation during RMT; (c) weakening of the grain boundary and (d) chemical heterogeneity at the grain boundary. During RMT, a fracture would occur whenever the stresses generated inside one grain could not be accommodated by neighbor grains that are already accommodating their own transformation stresses. The reader may also refer to aspects of fracture in SMA, including Cu-Al-Ni alloys, in the recent review by Baxevanis and Lagoudas [18].

The high elastic anisotropy in Cu-Al-Ni alloys creates a considerable stress concentration at the boundaries of differently oriented grains [16,17,19]. Fracture may then occur before or during the RMT, according to the alloy state of stresses. To improve the ductility of the polycrystalline Cu-Al-Ni alloys, several methods have been proposed, in association with the addition of quaternary elements, used as grain refiners. Among these methods, the plasma fusion technique is being explored as an alternative for fabrication of these alloys [20]. In spite of these efforts, actual modifications taking place in polycrystalline RMT-prone Cu-Al-Ni alloys subjected to cycling condition, which should occur in practice, have not yet been investigated. Therefore, the main objective of the present work was to investigate the changes in the structure and properties as well as in RMT parameters of a polycrystalline Cu-13.7%Al-4.0% Ni alloy after a load-free TCT within a temperature interval comprising the alloy critical transformation.

## 2. Experimental

A polycrystalline Cu-Al-Ni alloy, based on the intermetallic compound  $\text{Cu}_3\text{Al}$ , with weight content of 13.7%Al and 4.0%Ni (Cu-13.7Al-4Ni for short), produced by plasma fusion followed by injection molding in the Multidisciplinary Laboratory of Reactive Materials and Structures, at the Federal University of Campina Grande (UFCCG), Brazil, was investigated for the phase transformations and microstructural changes occurring under reversible martensitic transformation (RMT) after thermal cycling treatment (TCT).

The as-cast alloy ingot, a  $27 \times 25 \times 5$  mm bar, was heat treated to the stable  $\beta_1$  structure at 1125 K for 15 min followed by water quenching to room temperature (RT). This as-quenched ingot was sectioned in  $5 \times 5 \times 5$  mm specimens using a precision Miniton equipment. Each specimen was mirror-polished in a sequence including emery papers and diamond pastes. Specimens, were then subjected to load-free TCT's comprising heating up to 373 K, above the austenitic finishing temperature ( $A_f$ ), and cooling to 258 K, below the martensite finishing temperature ( $M_f$ ). The TCT's were performed in association with 1, 100, 200, 300, 400 and 500 cycles.

The alloy phases identification and semi-quantitative compositions were obtained at RT by X-ray diffraction (XRD) in a model XRD 7000 Shimadzu diffractometer operating with Cu-K $\alpha$  radiation in a  $2\theta$  interval from 25 to 100° and scanning steps of 0.03° with 3 s of accumulation. The phases semi-quantitative composition was estimated by means of the Origin™ program, which calculates the XRD peak integral as the phase volume fraction. Metallographic analysis was carried out in a model BX41M Olympus optical microscope. The average grains size was evaluated in the alloy initial state and after each TCT using the standard linear intercept method associated with a Scion™ image analyzer software. The morphological aspect and alloy microstructure were characterized for TCT's finishing with either ½ cooling cycle or ½ heating cycle, both at RT according to the procedure presented elsewhere [8,21–24].

The critical martensitic temperatures ( $M_s$ ,  $M_o$ ,  $M_p$ ,  $M_{of}$ ,  $M_f$ ) and austenitic (reversible) temperatures ( $A_f$ ,  $A_{of}$ ,  $A_p$ ,  $A_o$ ,  $A_s$ ) as well as hysteresis intervals and thermal effects associated with the alloy RMT were determined by differential scanning calorimetry (DSC) in a model DSC 296 TA Instrument for the initial state and after each TCT. The DSC tests were conducted in the temperature range of 173 K–423 K with a heating/cooling rate of 10 K/min under nitrogen. For determination of the RMT critical temperature, the well established tangent method [6,8,10,25] was applied. Vickers microhardness tests were performed in an equipment model HMV-2 Shimadzu.

## 3. Results and discussion

### 3.1. Initial as-quenched state

The polycrystalline Cu-13.7Al-4.0Ni alloy in its initial as-quenched condition displays the XRD pattern shown in Fig. 1. Four phases were identified and their semi-quantitative analyses are presented in Table 1. Although semi-quantitative, a standard deviation associated with the amount of phase was calculated from 3 different measurements of the area under each characteristic peak.

As for the phases shown in Table 1, one should remind that the  $\beta'_1$  martensite has an ordered  $\text{AlCu}_3$  type structure [26]; the  $\gamma'_1$  martensite an ordered  $\text{Cu}_3\text{Ti}$  type structure [27]; the  $\beta_1$  high temperature stable austenite, an ordered  $\text{BiF}_3$  type structure [28], and R, which is an intermetallic  $\text{Al}_7\text{Cu}_4\text{Ni}$ , has a metastable rhombohedral structure [8,21–24,29,30]. It has been reported that SME alloys, particularly those of the Cu-Al-Ni system may undergo either a single transformation ( $\beta_1 \leftrightarrow \beta'_1$  or  $\beta_1 \leftrightarrow \gamma'_1$ ) or a combined transformation ( $\beta_1 \leftrightarrow \beta'_1 + \gamma'_1$ ) depending on the alloy composition [31,32].

The DSC analysis of the as-quenched alloy in Fig. 2 shows that, under heating, the reverse austenite transformation occurred in the temperature interval from 291.8 K ( $A_s$ ) to 336.7 K ( $A_f$ ). This transformation was associated with an endothermic enthalpy of 9.3 J/g. The RMT under heating begins to occur at 312.2 K ( $A_o$ ) and goes through a peak at 318.2 K ( $A_p$ ) for a maximum heat flow. It clearly ends at 325.1 K ( $A_{of}$ ). Upon cooling, the direct transformation takes place between 323.5 K ( $M_s$ ) and 279.2 K ( $M_f$ ) with on-set peak of 309.5 K ( $M_o$ ) and off-set temperatures, 302.9 K ( $M_p$ ) and 293.1 K

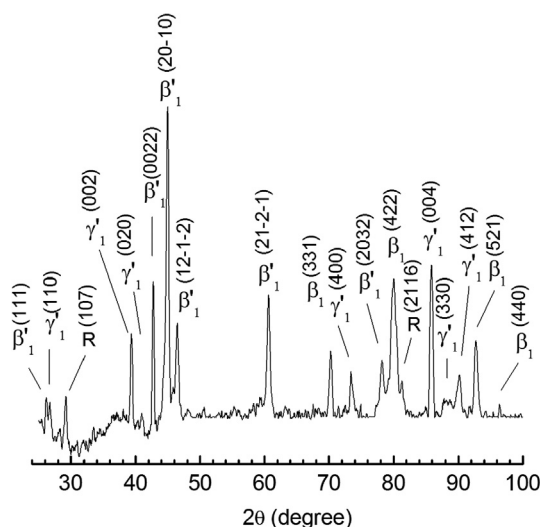
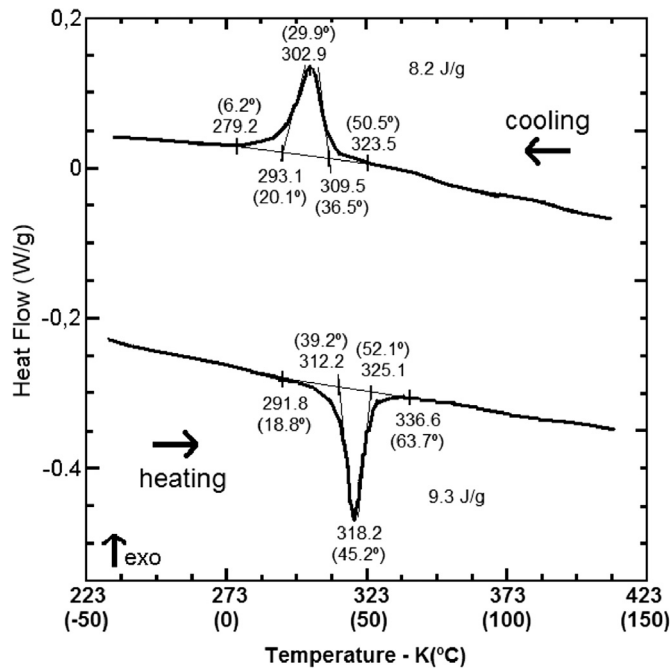


Fig. 1. XRD pattern of the polycrystalline Cu-13.7Al-4.0Ni alloy in as-quenched initial condition.

**Table 1**  
Semi-quantitative analysis of phases in initial as-quenched Cu-13.7Al-4.0Ni alloy.

Phase	Amount (vol. %)	Characteristic XRD peak
$\beta'_1$	$48 \pm 4$	(111), (0022), (20 $\bar{1}$ 0), (12 $\bar{1}$ 2), (21 $\bar{2}$ 1), (2032)
$\gamma'_1$	$23 \pm 2$	(110), (002), (020), (400), (004), (330), (412)
$\beta_1$	$26 \pm 2$	(331), (422), (521), (440)
R	$3 \pm 1$	(107), (2116)



**Fig. 2.** DSC curves during the first cycle of heating and cooling associated with RMT in the polycrystalline Cu-13.7Al-4.0Ni alloy.

( $M_{of}$ ), respectively, in association with an exothermic enthalpy of 8.2 J/g. For the thermal hysteresis measurement ( $\Delta T$ ), the difference between peak temperatures ( $A_p - M_p$ ) equal to 15.3 K was considered.

**Fig. 3** shows the morphological aspect of the polycrystalline Cu-13.7Al-4.0Ni alloy, observed in a section transversal to the samples longer direction. In its as-quenched initial state, **Fig. 3(a)**, the alloy microstructure reveals, with lower magnification, approximately equiaxed grains varying in size from 50 to 500  $\mu\text{m}$ . With higher magnification in **Fig. 3(b)**, a massive presence of martensite plates is seen inside each grain, with apparent random orientations. Both finer parallel needles and V-shaped wider laths are to be noticed. According to the literature [6] the fine needles and V-shaped laths

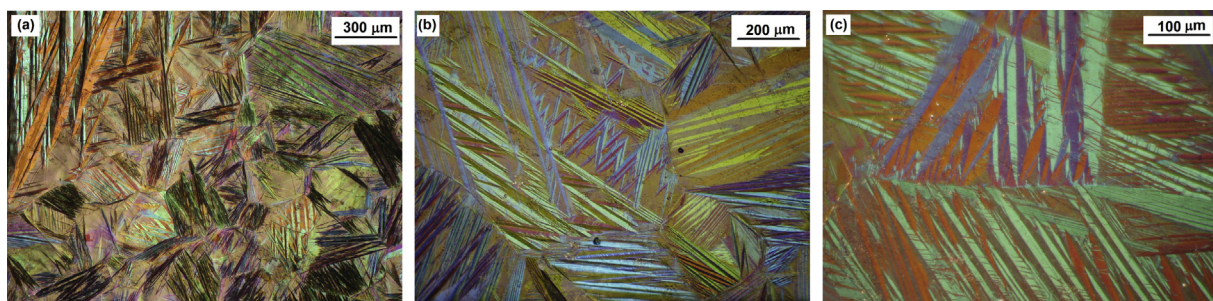


**Fig. 3.** Microstructure of the Cu-13.7Al-4.0Ni alloy in as-quenched initial state. Magnifications: (a) 50 $\times$ ; (b) 100 $\times$ ; and (c) 200 $\times$ .

are typical morphologies of  $\beta'_1$  and  $\gamma'_1$  martensites, respectively. These microstructural features are in agreement with the XRD results of **Fig. 1**.

**Fig. 4** shows the histogram of the grain size distribution obtained by the linear intercept method corresponding to eight 50  $\mu\text{m}$  intervals. A relatively normal dispersion and a main value of 162  $\mu\text{m}$  are associated with this histogram. Similar main diameter value was found in a previous work [33] on the same alloy. The alloy processing conditions were probably responsible for the greater dispersion found in grain size.

The Vickers microhardness obtained in 10 points on a flat and polished surfaces of the alloy was found as  $2.81 \pm 0.06$  GPa. This value is close to others reported for similar alloy [33–35] and the standard deviations indicate an uniform microhardness response of the as-quenched Cu-13.7Al-4.0Ni alloy.

### 3.2. XRD after TCT finishing with $\frac{1}{2}$ cooling cycle

**Fig. 5** shows the XRD patterns of the polycrystalline Cu-13.7Al-4.0Ni alloy subjected to load-free TCT's, up to 500 cycles, finishing with a  $\frac{1}{2}$  cooling cycle. **Table 2** presents a semi-quantitative analysis of the existing phases after TCT, by the characteristic peaks observed in **Fig. 5**. In this table one should note that for each phase several peaks were used to calculate the corresponding volume fraction. To avoid an overcrowded figure, the reader will notice that some peaks in **Table 2**, although existing, are not pointed out in **Fig. 5**.

As compared to the results in **Table 1** for the initial as-quenched alloy, the phase's amounts after one cycle finishing with  $\frac{1}{2}$  cooling

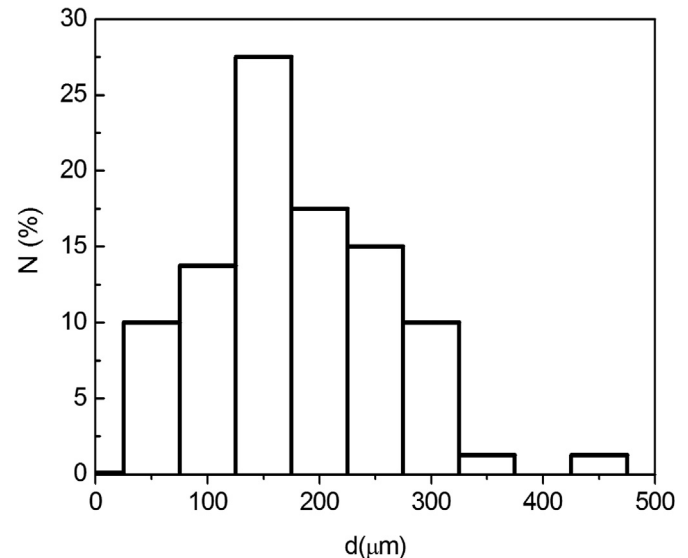


**Fig. 4.** Grain size distribution of the as-quenched polycrystalline Cu-13.7Al-4.0Ni alloy.

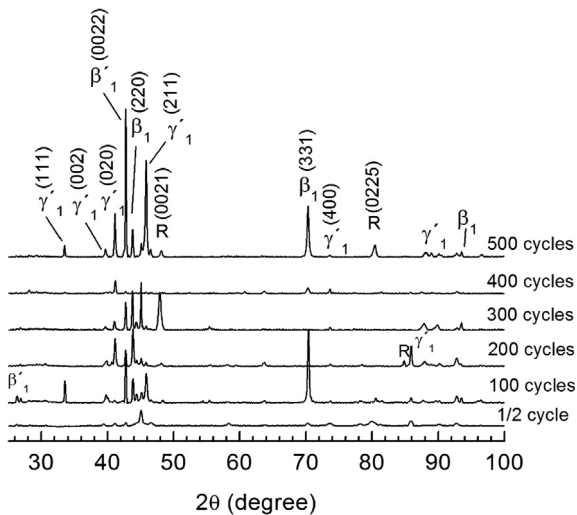


Fig. 5. XRD patterns of the Cu-13.7Al-4.0Ni alloy subjected to load-free TCT's of 100, 200, 300, 400 and 500, finishing with a  $\frac{1}{2}$  cooling cycle.

cycle in Table 2 are practically the same. This means that a single cycle is not enough to sensibly change the alloy structure. With increasing number of cycles, however, important changes occur. After 100 up to 500 cycles, the amount of  $\gamma'_1$  martensite significantly increases at the expenses of  $\beta'_1$ . Apparently, the accumulation of necessary dislocations to accommodate stresses caused by the cyclic martensite transformation favor a higher amount of  $\gamma'_1$  as the number of cycles increases. Indeed, it has been reported that accumulation of dislocations promotes changes in the martensite transformation parameters such as the value of critical RMT temperatures as well as variants and volume fraction of phases [6,36,37]. Additionally, the results in Table 2 indicate that phase R, first detected in small amount by only two planes, increases its participation with the number of cycles in association with many other crystallographic planes. The same rationale for  $\gamma'_1$  may apply for phase R.

Table 2  
Semi-quantitative analysis of phases in Cu-13.7Al-4.0Ni alloy after TCT finishing with  $\frac{1}{2}$  cooling cycle.

Number of cycles	Phase	Amount (vol. %)	Characteristic XRD peak
$\frac{1}{2}$	$\beta'_1$	45 ± 3	(111), (0022), (20 $\bar{1}$ 0), (12 $\bar{1}$ 2), (21 $\bar{2}$ 1), (2032)
	$\gamma'_1$	26 ± 3	(110), (002), (020), (400), (004), (330), (412)
	$\beta_1$	25 ± 3	(331), (422), (521), (440)
	R	4 ± 2	(107), (2116)
100	$\beta'_1$	18 ± 1	(111), (0022), (12 $\bar{1}$ 2), ( $\bar{2}$ 22), (2032)
	$\gamma'_1$	34 ± 2	(110), (111), (002), (020), (012), (211), (400), (004), (330), (014), (412)
	$\beta_1$	42 ± 1	(220), (222), (331), (521), (440)
	R	6 ± 2	(1016), (0021), (1025), (0225)
200	$\beta'_1$	8 ± 2	(0022), ( $\bar{2}$ 22), (2032)
	$\gamma'_1$	49 ± 1	(110), (002), (020), (012), (211), (212), (221), (400), (004), (330), (412)
	$\beta_1$	26 ± 1	(200), (220), (521)
	R	17 ± 1	(107), (0114), (1016), (0021), (1025), (309)
300	$\beta'_1$	12 ± 2	(0022), ( $\bar{2}$ 22)
	$\gamma'_1$	33 ± 1	(002), (212), (211), (1 $\bar{1}$ 0), ( $\bar{4}$ 00), (330), (014)
	$\beta_1$	16 ± 1	(220), (521)
	R	39 ± 2	(0114), (1016), (0021)
400	$\beta'_1$	17 ± 2	(111), (202), (0022), (20 $\bar{1}$ 0), (12 $\bar{1}$ 2), (21 $\bar{2}$ 1), (1123), ( $\bar{2}$ 22)
	$\gamma'_1$	46 ± 2	(011), (111), (002), (020), (211), (022), (400), (004), (330), (014)
	$\beta_1$	23 ± 2	(200), (400), (331), (521)
	R	14 ± 2	(107), (1016), (0021), (1019), (0213), (2017), (300)
500	$\beta'_1$	22 ± 2	(0022), (12 $\bar{1}$ 2)
	$\gamma'_1$	46 ± 1	(111), (002), (020), (012), (211), (330), (014), (412)
	$\beta_1$	25 ± 1	(220), (331), (521), (440)
	R	7 ± 2	(0021), (0225)

### 3.3. XRD after TCT finishing with a $\frac{1}{2}$ heating cycle

Fig. 6 presents the XRD patterns of the polycrystalline Cu-13.7Al-4.0Ni alloy subjected to load-free TCT's, up to 500 cycles, finishing with a  $\frac{1}{2}$  heating cycle. Table 3 presents a semi-quantitative analysis of the existing phases from peaks in Fig. 6 following the same procedure described for Table 2. Similar results presented in this table, related to the tendency of changes in the amount of phases, can be observed in Table 3. Therefore, one should also expect that TCT's finishing with  $\frac{1}{2}$  heating cycles are also affected by changes in martensite transformation due to accumulation of dislocations [6,36,37]. This is, to a certain extent, a surprising result. Previous works [8,10,22–24] on the influence of TCT in a monocrystalline Cu-Al-Ni alloy, subjected to experimental procedures similar to the present work, revealed that the way the TCT finishes with  $\frac{1}{2}$  cycle, either cooling or heating, alters the participation of the different phases. The polycrystalline structure of the Cu-13.7Al-4.0Ni alloy, on the contrary, has a common transformation, probably  $\beta_1 \leftrightarrow \gamma'_1 + \beta'_1$ , involving the same relatively larger amounts of  $\gamma'_1$  martensite with increasing number of cycles, regardless the way TCT finishes. Moreover, since the XRD were performed at RT within the RMT interval, it is also expected a common transformation behavior of phase R in more complex  $\beta_1 \leftrightarrow R \leftrightarrow \gamma'_1 + \beta'_1$  reactions [35].

Fig. 7 shows the variation of phasic volume fraction obtained from a semi-quantitative analysis of XRD peaks in Figs. 1, 5 and 6, as function of the number of cycles. The solid and dashed lines correspond to TCT's finishing with  $\frac{1}{2}$  cooling and heating cycles, respectively. In Fig. 7(a) it is observed a tendency to increase  $\gamma'_1$  with respect to the high temperature stable  $\beta_1$ . It is then suggested that multiple thermal cycles might accentuate the direct martensite transformation  $\beta_1 \rightarrow \gamma'_1$ . As for the intermediate R phase, Fig. 7(b), it tends to increase and become with a volume fraction similar to  $\beta'_1$ . The reason for this tendency of R, initially in smaller amount, is not yet clear.

### 3.4. DSC analysis after TCT

Fig. 8 depicts the DSC curves associated with: (a) cooling and (b)

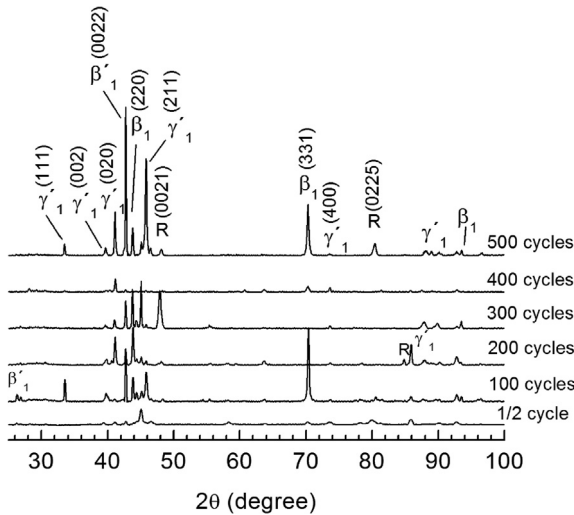


Fig. 6. XRD patterns of the Cu-13.7Al-4.0Ni alloy subjected to load-free TCT's of 100, 200, 300, 400 and 500 finishing with a  $\frac{1}{2}$  heating cycle.

heating, within the interval of 223 K–423 K for the polycrystalline Cu-13.7Al-4.0Ni alloy. In this figure, vertical dotted lines indicate the limits (maximum temperature) for the peaks corresponding to the martensitic transformation ( $M_p$ ) on cooling and the reversible austenitic transformation ( $A_p$ ) upon heating. It should be noticed that, with accumulation of 300 cycles, the values of  $M_p$  and  $A_p$  are slightly displaced to lower temperatures, 8.2 and 6.2 K, respectively, in comparison with the as-quenched initial condition. For higher number of cycles, 400 and 500 in Fig. 8, there is a subtle displacement ( $\sim 2$ –3 K) of  $M_p$  and  $A_p$  to higher temperatures.

Fig. 9 shows the variation of the RMT critical temperatures, during (a) heating and (b) cooling, with the number of TCT cycles. Except for the slight displacement to lower temperature of some parameter, specially at 300 cycles as already mentioned for  $M_d$  and  $A_p$  in Fig. 8, no general trend exist with increasing number of cycles. However, it is important to note that  $M_f$  and  $A_s$  are sensibly

reduced, by approximately 10 K, from the as-quenched initial state to 500 cycles. These are interesting results that not only influence the hysteresis behavior of the alloy but could also be affected by small amounts of elements, such as Mn and Fe. Indeed, a recent work of Mazze et al. [38] on the thermal stability of Cu-Al-Ni-Mn SMA reported an increase in  $A_s$  and  $A_f$  associated with increasing annealing time and temperature. One may infer that cycling in the absence of Mn could affect the transformation parameters in a reverse way. Benke and Mertinger [39] found in a Cu-Al-Ni-Mn-Fe SMA that different martensite variants were formed after every thermal cycle. However, transformations were not accompanied by observable plastic deformation. As further discussed, evidences of plastic deformation were observed in the present work.

Fig. 10 shows the change in the hysteresis,  $\Delta T$ , and transformation enthalpy with the number of TCT cycles. The value of  $\Delta T$  in the as-quenched initial state, Fig. 10(a), sensibly increases from 15.3 K to 17.4 K after 100 cycles, which is a consequence of the maximum in  $A_s$  displayed in Fig. 9. At higher number of cycles, Fig. 10(a),  $\Delta T$  remained practically constant. In addition to changes in  $\Delta T$  and critical temperatures, the reader should notice in Fig. 9 an increase in the total RMT interval after 500 cycles. Indeed, the values of  $M_s - M_f = 35$  K and  $A_f - A_s = 45$  K in the initial state, change to 50 and 52 K, respectively, after 500 cycles. The literature [6,8–10,35] indicates that defects accumulated after each cycle are responsible for the increase in the transformation interval by making difficult the mechanism for RMT. It is herein proposed that defects such as dislocations are accumulated as a consequence of internal stresses generated by elastic deformation of the lattice associated with transformation. The stress field acts as a barrier and causes the martensitic reaction  $\beta_1 \rightarrow R \rightarrow \gamma_1 + \beta'_1$  to occur at lower temperatures. This continuously retards the transformation finishing,  $M_f$  in Fig. 9(a), with accumulation of cycles.

As for the transformation enthalpies, Fig. 10(b) indicates only a slight difference between the direct ( $E_M$ ) and reverse ( $E_A$ ) transformations. Moreover, both enthalpies are practically not affected by the number of cycles. This is apparently an indication that the alloy thermodynamic state is not influenced either by the direction of transformation or the number of TCT cycles.

Table 3

Semi-quantitative analysis of phases in Cu-13.7Al-4.0Ni alloy after TCT finishing with  $\frac{1}{2}$  heating cycle.

Number of cycles	Phase	Amount (vol. %)	Characteristic XRD peak
$\frac{1}{2}$	$\beta'_1$	45 ± 2	(111), (0022), (20 $\bar{1}$ 0), (12 $\bar{1}$ $\bar{2}$ )
	$\gamma_1$	28 ± 1	(011), (002), (020), (212), (221)
	$\beta_1$	24 ± 2	(400), (331)
	R	3 ± 1	(018)
100	$\beta'_1$	17 ± 3	(0022), (20 $\bar{1}$ 0), ( $\bar{2}$ 22)
	$\gamma_1$	61 ± 2	(002), (201), (020), (211), (400), (004), (330), (412), (011), (212), (221), (122)
	$\beta_1$	16 ± 2	(220), (200), (222), (331), (521), (111)
	R	6 ± 1	(1016), (0021), (107), (0225), (309)
200	$\beta'_1$	18 ± 0	(20 $\bar{2}$ 4)
	$\gamma_1$	62 ± 2	(111), (201), (211), (330), (412)
	$\beta_1$	17 ± 2	(220), (222), (331), (422), (521)
	R	3 ± 2	(0225), (309)
300	$\beta'_1$	20 ± 3	(0022), ( $\bar{2}$ 22), (2032)
	$\gamma_1$	27 ± 2	(002), (020), (012), (400), (213), (402), (022)
	$\beta_1$	10 ± 3	(200), (220), (521)
	R	43 ± 1	(107), (0021), (0225), (1016)
400	$\beta'_1$	7 ± 2	(0022), (2032)
	$\gamma_1$	63 ± 4	(011), (002), (020), (211), (400), (330), (014)
	$\beta_1$	8 ± 2	(220), (331), (521)
	R	22 ± 2	(107), (0021), (0225), (309)
500	$\beta'_1$	8 ± 1	(0022), (12 $\bar{1}$ $\bar{2}$ )
	$\gamma_1$	55 ± 1	(111), (002), (020), (012), (211), (011), (212), (330), (014), (412)
	$\beta_1$	27 ± 1	(220), (400), (331), (521)
	R	10 ± 1	(1016), (0021), (0225)

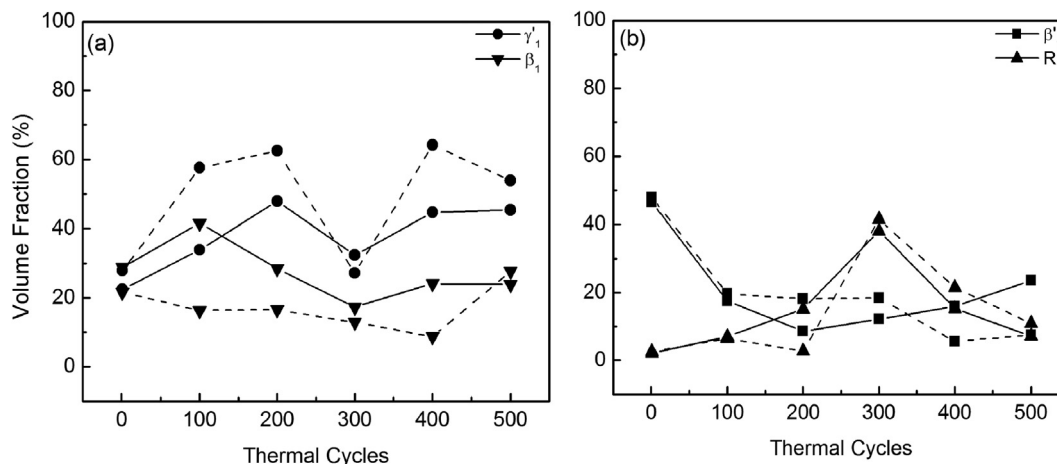


Fig. 7. Variation of the volume fraction of phases obtained from XRD after TCT's finishing with  $\frac{1}{2}$  cooling cycle (solid line) and  $\frac{1}{2}$  heating cycle (dashed line): (a)  $\gamma'_1$  and  $\beta_1$ ; (b)  $\beta'_1$  and R phases.

### 3.5. Morphological changes with TCT

The structural morphology of the polycrystalline Cu-13.7Al-4.0Ni alloy with the number of load-free TCT cycles, finishing with  $\frac{1}{2}$  cooling cycle, is shown in Fig. 11. It is well known that the direct transformation introduces the characteristic martensitic relief on a mirror-polished surface of SME alloys [5,6]. These relief marks are usually referred as plate, lath, lamella or needle and were also observed, Fig. 3, in the alloy as-quenched initial condition. For each number of cycles in Fig. 11, two different magnifications illustrate the typical morphology. The lower magnification pictures, Fig. 11 (a), (c), (e), (g), and (i), correspond to the same observed region. This permits to infer that both the type and amount of marks are apparently similar, regardless the number of cycles. However, a close look at the same region with higher magnification, Fig. 11(b), (d), (f), (h), and (j), reveals the development of additional very thin lines that might result from dislocation slip causing irreversible plastic deformation. This could be related to the mechanism responsible for the displacement of the RMT critical temperatures shown in Figs. 8 and 9. However, the existence of Mn and Fe in the Cu-Al-Ni SMA may hinder plastic deformation [39].

In terms of the specific morphology, it is known [10,35] that the high temperature stable  $\beta_1$  constitutes the matrix in Fig. 11. The needles are characteristic of  $\beta'_1$  while the crossing (V-shaped) lamellae are typical of  $\gamma'_1$ . These phases identified by their morphologies are also detected by XRD in Figs. 5 and 6. Two factors were found to affect the alloy morphology. First, owing to self-accommodation, some martensite variants may be eliminated by others as suggested in the work of Benke and Mertinger [39]. In principle, for each grain, 24 variants are expected to be activated [6,19]. The constraint imposed by neighboring grains not only limits this activation but also might change or eliminate the active ones with the cycling treatments. Second, above 200 cycles, the relatively greater participation of the R and  $\beta_1$  phases, Figs. 5 and 6, tends to decrease the amount of needles ( $\beta'_1$ ) and V-shaped ( $\gamma'_1$ ) marks. This is particularly accentuated for the 300 cycles, as seen in Fig. 11 (e) and (f). The reader should be aware that the presence of the R phase cannot be correlated to a specific morphology. This phase is coherent with  $\beta'_1$  and can only be detected by XRD [35].

The aforementioned factors combined with the observed very thin slip lines, responsible for accumulation of plastic deformation after each cycle, contribute to retard the RMT, Fig. 9, as a consequence of TCT's.

Another interesting phenomenon observed for the first time

was the pullout of small grains. The sequence of micrographs with relatively low magnification in Fig. 11(a), (c), (e) and (g) shows, step by step, the gradual decohesion of a grain (pointed by arrows) until its final pullout in Fig. 11(i). It is proposed that the mechanical constraints imposed by neighbor grains and weakening of grain boundaries [16,17] be responsible for this phenomenon. Indeed, the multiple transformation and complex activation of martensite variants, particularly in the large grain shown at the bottom left in Fig. 11, apparently caused a state of stress enough to break the atomic bonding of the small arrow-pointed small grain. In spite of the solid polycrystalline structure, this small grain on the specimen surface, without an outside counter reaction, was pulled out and left a corresponding black hole (Figs. 11(i) and 12). The statistics (frequency) of this phenomenon and quantitative evaluation of local grain boundary stresses need to be further evaluated.

Regarding the grain participation, Fig. 13 shows the distribution of the alloy average grain size measured by the line intercept method in metallographic samples associated with the distinct levels of TCT. For each number of cycles, including the initial zero cycle, a relatively broad grain size interval of 50–450  $\mu\text{m}$  corresponds to the bounds of an approximately normal distribution. As shown in Fig. 13 the mean value for each number of cycles tends to increase from 162  $\mu\text{m}$ , initial state in Fig. 4, up to 211  $\mu\text{m}$  for 300 cycles. A decrease to 175  $\mu\text{m}$  for 500 cycles indicates that the RMT associated with TCT is capable of introducing changes in the grain structure. This behavior has not yet been reported and the reason appears to be the constraints imposed by each grain in its neighbors due to repeated transformations. This contributes to change not only the size distribution, Fig. 13, but also to pull small grains, Figs. 11(i) and 12, out of the polycrystalline structure. As for the top mean value for 400 cycles, the reason is not yet clear but the maximum participation of the  $\gamma'_1$  phase, Table 3, might be associated with the highest stress field caused by the complex transformation.

### 3.6. Microhardness after TCT

The variation of the microhardness of the polycrystalline Cu-13.7Al-4.0Ni alloy with the number of load-free TCT cycles is shown in Fig. 14. In this figure, each point and corresponding error bar represent the average and standard deviation of 10 tests performed in a flat and polished cross section. Tests were carried out in samples after TCT finishing with  $\frac{1}{2}$  cooling cycle corresponding to the XRD in Fig. 5 and the microstructures in Fig. 11. As

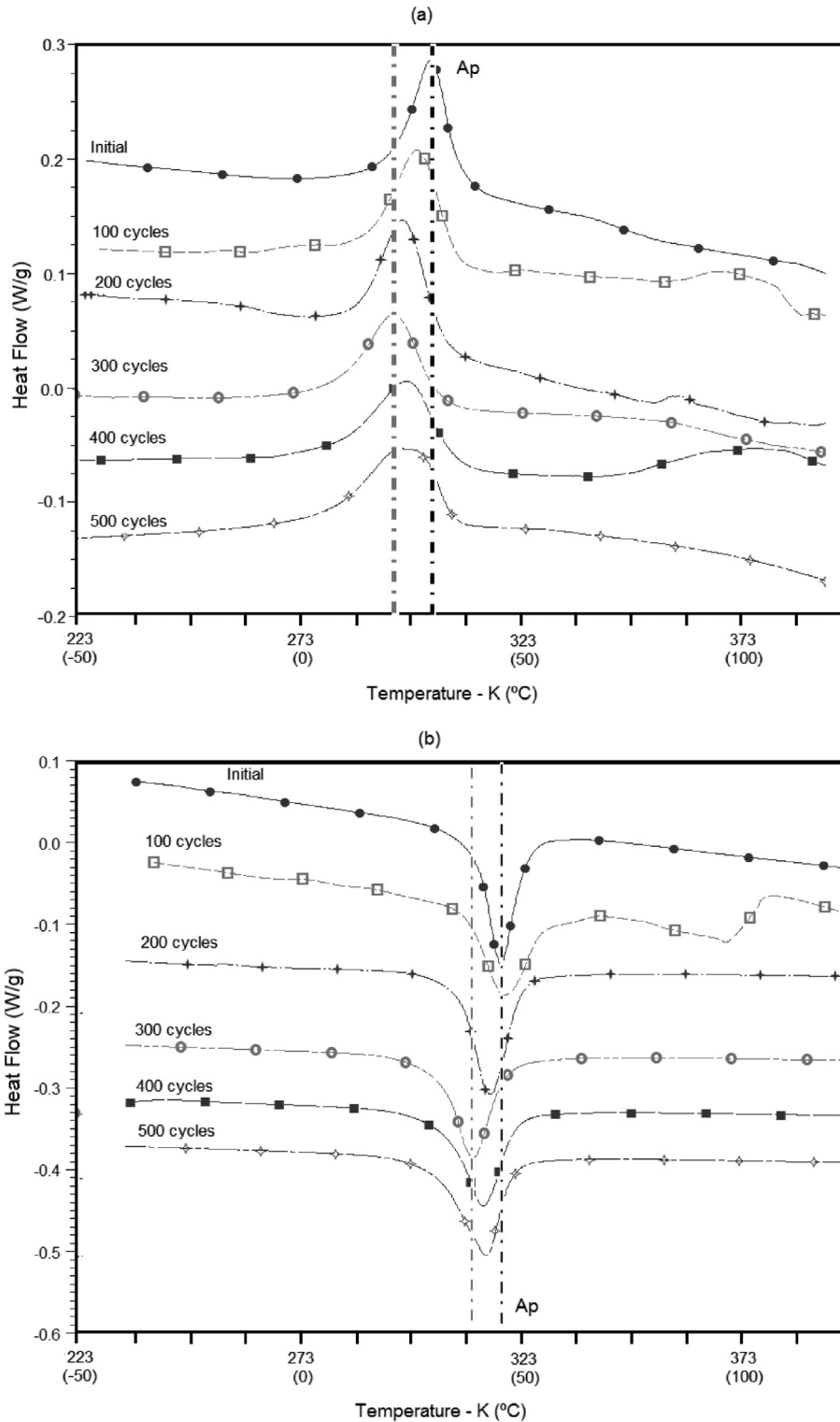


Fig. 8. –DSC curves for the polycrystalline Cu-13.7Al-4.0Ni alloy after TCT's corresponding to different number of cycles during: (a) cooling and (b) heating.

aforementioned, the microhardness of the as-quenched initial condition was found as  $2.81 \pm 0.06$  GPa. This value in Fig. 14 decrease to  $2.42 \pm 0.09$  GPa for 200 cycles and then, within the error bars, remains practically constant up to 500 cycles. It is clear in this figure that the as-quenched initial state of the alloy, with phasic composition presented in Table 1, reduces its hardness after 200 cycles. One possibility for this behavior could be the higher

hardness of  $\beta'_1$  martensite, which corresponds to 48% of the initial state. After 200 cycles, Table 2, a significant reduction of  $\beta'_1$  to only 8.6%, together with a relative increase in the amount of phases  $\gamma'_1$  and  $\beta_1$ , with comparatively lower hardness, could explain the results in Fig. 14. Moreover, the raise in  $\beta'_1$  content to 23.5%, Table 2, for 500 cycles also agrees with the tendency of a slightly greater hardness in Fig. 14. In addition to the specific hardness contribution

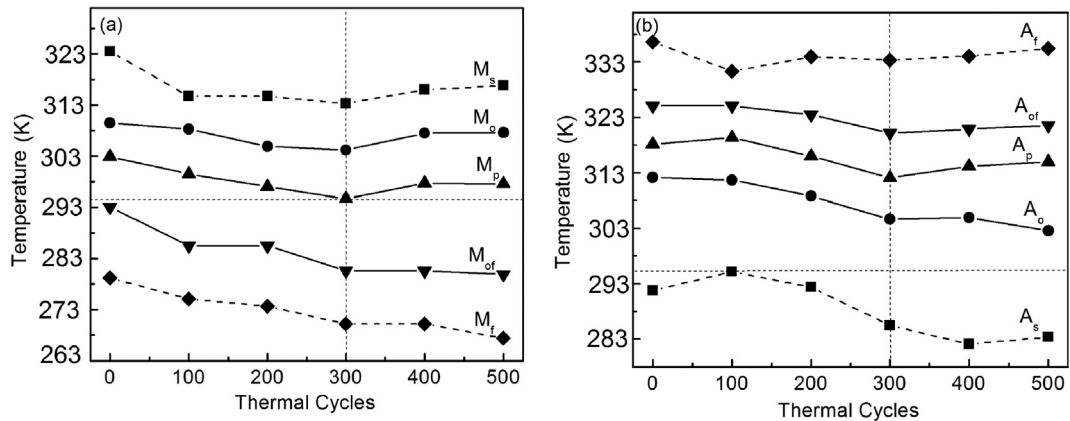


Fig. 9. Variation of the critical RMT temperatures, obtained by DSC for the polycrystalline Cu-13.7Al-4.0Ni alloy, with the number of cycles for: (a) cooling and (b) heating.

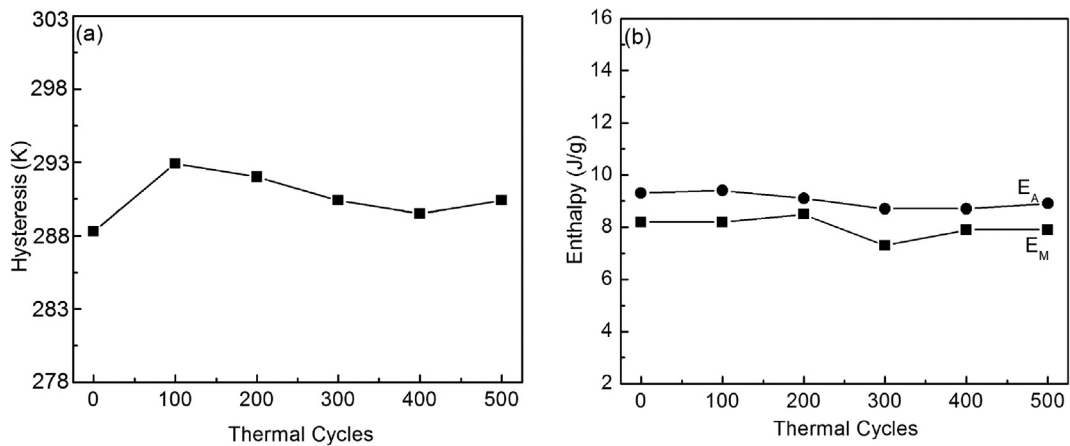


Fig. 10. Variation of the RMT hysteresis (a) and enthalpy (b) with the number of cycles for the polycrystalline Cu-13.7Al-4.0Ni alloy.

of each phase, other already discussed factors such as accumulation of defects, elimination of martensite variants by self-accommodation and development of internal stress field may play a role in changing the hardness of the alloy subjected to RMT under increasing TCT's.

### 3.7. Contribution of the $\gamma'_1$ martensite

An important point raised by the results of the present work is the difference between single crystal and polycrystalline alloys. Works on both thermal and pseudoelastic (mechanically) cycling, up to 2700 cycles, of RMT-prone Cu-Al-Ni SMA single crystals conducted by Gastien et al. [12–14] revealed an inhibition of the  $\gamma'_1$  martensite with increasing number of cycles. By contrast, in the thermal-only cycling up to 500 cycles of the present work, the  $\gamma'_1$  tends to increase from 1 to 200 cycles, Tables 2 and 3, as evaluated from XRD patterns in Figs. 5 and 6. A decreased occurred from 300 cycles, due to a maximum participation of the coherent R phase, returning to higher values of  $\gamma'_1$  for 400 and 500 cycles.

In the case of load-assisted pseudoelastic cycling of a single crystal alloy, not showing  $\gamma'_1$  quantitative values, Gastien et al. [12–14] results on the evolution of hysteresis by electrical resistance apparently indicate inhibition from 100 cycles upwards. This was attributed to the introduction of defects during cycling. Based on a microscopic model, Gastien et al. [12–14] concluded that both the generation of stacking faults and the difficulty to create an undistorted habit plane inhibit the formation of the  $\gamma'_1$  structure.

On the contrary,  $\beta'$  was not found to be affected by these mechanisms and the  $\beta_1 \leftrightarrow \beta'_1$  transformation would prevail with cycling.

In principle, the increase in  $\gamma'_1$  obtained in Tables 2 and 3 could be rationalized as being a consequence of load-free, i.e. just thermal-cycling. However, in another thermal-only cycling experimental investigation, Gastien et al. [12–14] also observed inhibition of  $\gamma'_1$  formation. The authors claimed that their proposed model could also be used for thermal-only cycling because the generated dislocations are similar to those observed in load-assisted cycled single crystals. A recent work [8] also obtained evidence of  $\gamma'_1$  inhibition by XRD in thermal-only cycling of a monocrystalline Cu-13.7Al-4.2Ni alloy.

To clarify this apparent controversy, it is proposed that the increase in  $\gamma'_1$ , Tables 2 and 3, up to 200 cycles found in the present work is due to the alloy polycrystalline structure. From a simple thermodynamic point of view, one cannot explain the predominance of  $\gamma'_1$  over  $\beta'_1$ , since the difference in the free energy of both martensitic structures is very small and the crystallographic transformation from one into another is possible to occur by simple atomic redistribution [36,40]. Indeed, the present as-quenched polycrystalline alloy, Table 1, as well as single crystal alloys in their first thermal or pseudoelastic cycle showed both  $\gamma'_1$  and  $\beta'_1$  martensites [8,12–14].

The existence of several grains with distinct orientations allows martensitic variants to be transformed along many space directions in a polycrystalline structure. In principle, martensitic transformation might occur by elastic (Bain) distortion and shear

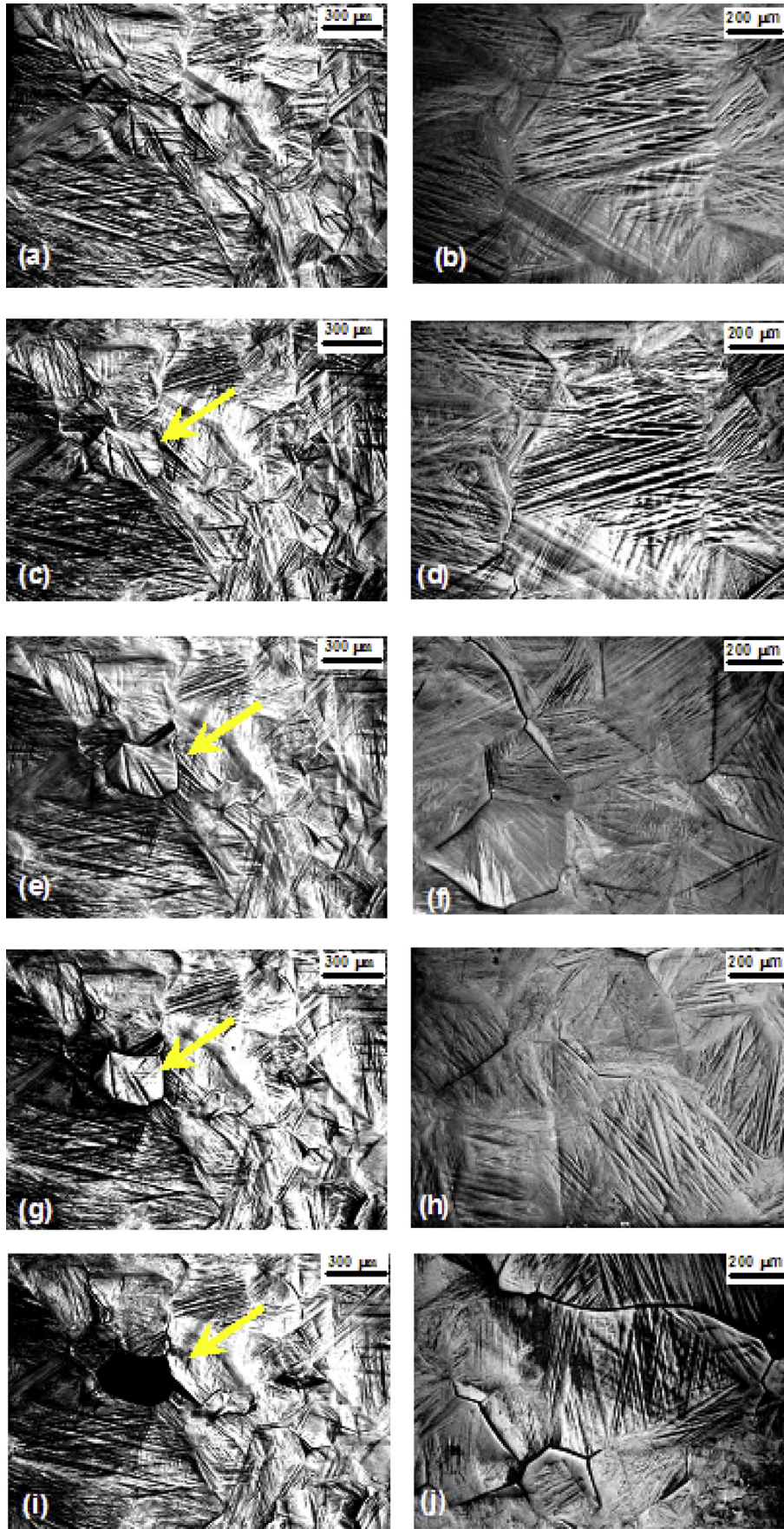


**Fig. 11.** Microstructure of the polycrystalline Cu-13.7Al-4.0Ni alloy after TCT's corresponding to: 100 (a) and (b); 200 (c) and (d); 300 (e) and (f); 400 (g) and (h); and 500 (i) and (j) cycles.

deformation (twinning) with no need of dislocations [41]. This may be the case of some grains in the present polycrystalline alloy, Fig. 11, for which Gastien et al. [12–14] mechanism of  $\gamma'_1$  inhibition might not be applied. For other grains, dislocations may be generated after each RMT cycle to accommodate eventual stress fields caused by phase transformations. Therefore, in polycrystalline alloys,  $\gamma'_1$  can never be totally inhibited. The question is then why the amount of  $\gamma'_1$  would increase, at least up to 200 cycles, as presented in Tables 2 and 3. A possible reason is the formation of the R phase, which is coherent with  $\beta'_1$ , and certainly requires its own transformation energy. This competes against the complex condition of  $\gamma'_1$  transformation, which is easy in some grains and inhibited in others. As a consequence,  $\beta'_1$  might also suffer partial inhibition, Table 3, with TCT's finishing with  $\frac{1}{2}$  heating cycle.

#### 4. Final remarks

The XRD results, Figs. 1, 5 and 6, combined with DSC analysis, Figs. 2 and 8, and microstructure observation, Figs. 3 and 11, revealed a complex sequence of phase transformations during load-free thermal cycling of the polycrystalline Cu-13.7Al-4.0Ni alloy subject to RMT. Although only four phases were involved in the transformations, a complex array of martensite variants is formed through the possible  $\beta_1 \leftrightarrow R \leftrightarrow \gamma'_1 + \beta'_1$  reactions. Moreover, the participation of martensite variants in every grain, Fig. 11, was also modified with the evolution of cycles [29]. Elimination of some variants by the stress fields of others as well as the accumulation of irreversible plastic deformation associated with very thin slip lines, added to the transformation complexity. As a consequence, for the first time, it was observed the phenomenon of a surface grain pullout, Figs. 11(i) and 12, out of the polycrystalline structure, in association with a sensible change in mean grain size, Fig. 13, with TCT's.

For SME applications, the interval of RMT and its relation to room temperature (RT) are of practical interest. In the present work RT was set as 294 K, indicated as the horizontal dotted-line in Fig. 9. One should notice that the peak of martensite transformation ( $M_d$ ) upon cooling, Fig. 9(a), is closer to RT and, for 300 cycles (vertical line), actually coincides with RT at which temperature the XRD analysis, Fig. 5, was performed. In this analysis, Table 2, the  $\gamma'_1$  martensite marked increased with the number of cycle and the R phase shows a maximum amount for 300 cycles. It is herein proposed that the greater participation of  $\gamma'_1$  and R is responsible for the enlargement of the RMT interval, Fig. 9(a) as the cycling treatment proceeds. A similar rationale applies upon heating, Fig. 9(b), for the reversible phasic reactions. In this case, however, RT (horizontal dotted line) is closer to the beginning ( $A_s$ ) of transformation. The participation of  $\gamma'_1$  and R, especially at 300 cycles, Table 3, is dominant.

#### 5. Conclusions

The polycrystalline Cu-13.7 wt%Al-4.0 wt%Ni alloy suffers with load-free thermal cycling treatment (TCT) a complex sequence of reversible martensitic transformations (RMT)  $\beta_1 \leftrightarrow R \leftrightarrow \gamma'_1 + \beta'_1$ , in which the amount and microstructure of the phases are very sensitive to the number of cycles.

TCT's promote changes in the RMT critical temperatures, such as their displacement to lower temperatures as well as the broadening of the total transformation interval. The RMT hysteresis sensibly increases with the first 100 cycles from the as-quenched initial state but the transformation enthalpy was practically unchanged with the number of cycles.

The alloy structural changes finishing the treatment with a  $\frac{1}{2}$  heating cycle (RT  $\rightarrow$  373 K  $\rightarrow$  RT) revealed a good association with

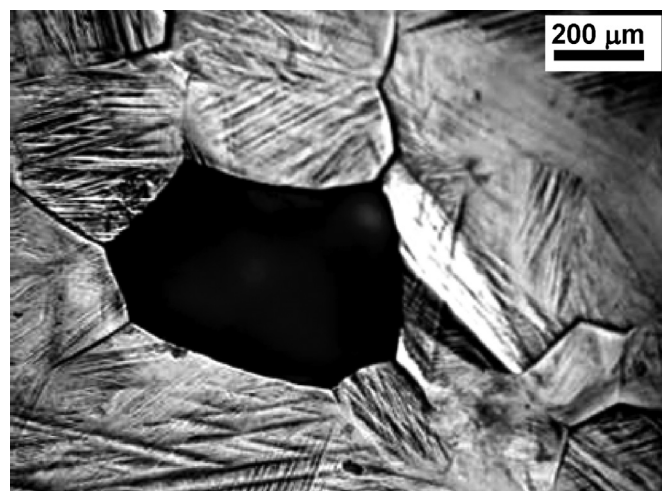


Fig. 12. Black hole corresponding to the ejection of a grain in the polycrystalline Cu-13.7Al-4.0Ni after 500 cycles.

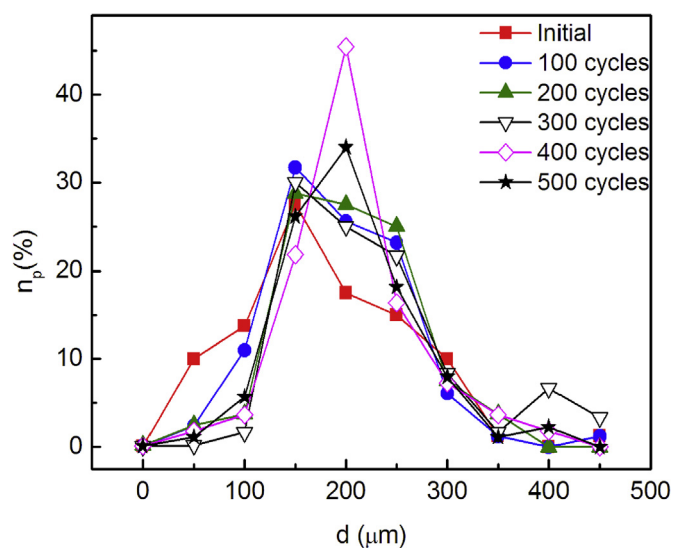


Fig. 13. Grain size distribution in the polycrystalline Cu-13.7Al-4.0Ni after different TCT's.

the direct RMT critical temperatures. The field for the existence of a greater amount of the martensitic  $\beta'_1$  phase, is located next to or below the end of the intensive direct RMT (below  $M_{of}$ ). Above this temperature, a greater participation of the  $\gamma'_1$  martensite as well as the presence of the intermediate R phase are observed.

Reversible martensitic transformations and structure reorientations in each grain of the polycrystalline alloy, during multiple thermal cycles, in addition to the high RMT anisotropy, typical of the Cu-Al-Ni system alloys, justifies the grain boundary fracture. The high stress concentration at the boundaries of differently oriented grains is capable of pulling out small surface grains, most notably after 500 cycles.

The alloy displays in its initial state a Vickers microhardness value of  $2.81 \pm 0.06$  GPa, which is reduced to  $2.37 \pm 0.05$  GPa at 300 cycles, with appearance of the intermediate R phase. Beyond this level of cycling treatment, a more resistant structure to further accumulation of irreversible deformation is formed.

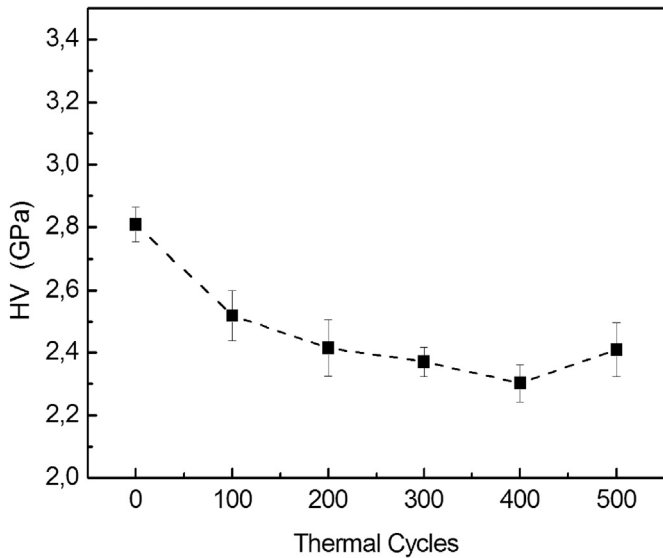


Fig. 14. Variation of the microhardness with number of cycles for the polycrystalline Cu-13.7Al-4.0Ni alloy.

### Acknowledgements

The authors thank the Brazilian Agencies FAPERJ (E-26/110.814/2008-APQ1), CAPES and CNPq. It is also acknowledged the LAM-MEA/UFCG student Antônio Aristófanés da Cruz Gomes for providing the preparation of the alloy.

### References

- [1] K. Otsuka, H. Sakamoto, K. Shimizu, Successive stress-induced martensitic transformations and associated transformation pseudoelasticity in Cu-Al-Ni alloys, *Acta Metall.* 27 (1979) 585–601.
- [2] G.V. Kurdyumov, L.G. Khandros, Thermoelastic equilibrium on martensitic transformations, translated and reprinted from, *Dokl. Akad. Nauk. SSSR* 66 (1949) 211–214.
- [3] V. Novák, P. Sittner, D. Vokonn, N. Zárubová, On the anisotropy of martensitic transformations in Cu-based alloys, *Mater. Sci. Eng. A* 273–275 (1999) 280–285.
- [4] N. Zárubová, J. Gemperlová, V. Gartnerová, A. Gemperle, Stress-induced martensitic transformations in a Cu–Al–Ni shape memory alloy studied by in situ transmission electron microscopy, *Mater. Sci. Eng. A* 481–482 (2008) 457–461.
- [5] J. Perkins, Shape memory effects and applications, in: *Proceeding International Conference, Toronto-Ontario, Canada, 1975*, 583pp.
- [6] K. Otsuka, C.M. Wayman, *Shape Memory Materials*, Cambridge University Press, Cambridge, 1999, 300pp.
- [7] S. Pulnev, V. Nikolaev, A. Priadko, A. Rogov, I. Vahhi, Phase transformation behavior of Ti50Ni30Cu20 shape memory alloys, *J. Mater. Eng. Perform.* 20 (2011) 497–499.
- [8] E.C. Pereira, L.A. Matlakhova, A.N. Matlakhov, C.Y. Shigue, S.N. Monteiro, Physical and structural characterization of a monocrystalline Cu-13.7Al-4.2Ni alloy subjected to thermal cycling treatments, *Metall. Mater. Trans. A* 45 (2014) 1866–1875.
- [9] M. Morin, F. Trivero, Influence of thermal cycling on the reversible martensitic transformation in a Cu-Al-Ni shape memory alloy, *Mater. Sci. Eng. A* 196 (1995) 177–181.
- [10] R.J. Silva, L.A. Matlakhova, E.C. Pereira, A.N. Matlakhov, S.N. Monteiro, R.J.S. Rodríguez, Thermal cycling treatment and structural changes in Cu-Al-Ni monocrystalline alloys, *Mater. Sci. Forum* 514–516 (2006) 692–696.
- [11] A. Ibarra, P.P. Rodríguez, V. Recarte, J.I. Pérez-Landazábal, M.L. Nó, J. San Juan, Internal friction behaviour during martensitic transformation in shape memory alloys processed by powder metallurgy, *Mater. Sci. Eng. A* 370 (2004) 492–496.
- [12] R. Gastien, C.E. Corbellani, M. Sade, F.C. Lovey, A  $\sigma$ - $T$  diagram analysis regarding the  $\gamma'$  inhibition in  $\beta \leftrightarrow \beta' + \gamma'$  cycling in CuAlNi single crystals, *Scr. Mater.* 54 (2006) 1451–1455.
- [13] R. Gastien, C.E. Corbellani, M. Sade, F.C. Lovey, The inhibition of  $\gamma'$  martensite in  $\beta \leftrightarrow \beta' + \gamma'$  cycling in Cu–Al–Ni single crystals, *Mater. Sci. Eng. A* 481–482 (2008) 518–521.
- [14] R. Gastien, M. Sade, F.C. Lovey, Interaction between martensitic structure and defects in  $\beta \leftrightarrow \beta' + \gamma'$  cycling in CuAlNi single crystals. Model for the inhibition of  $\gamma'$  martensite, *Acta Mater.* 56 (2008) 1570–1576.
- [15] V.E.A. Araujo, R. Gastien, E. Zelaya, J.I. Beiroa, I. Corro, M. Sade, F.C. Lovey, Effects of martensitic transformations and the microstructures of CuAlNi single crystals after ageing at 473K, *J. Alloys Compd.* 64 (2015) 155–161.
- [16] H. Sakamoto, K. Shimizu, K. Otsuka, Fatigue properties associated with cyclic transformation pseudoelasticity of CuAlNi alloy single crystals, *Trans. Jpn. Inst. Met.* 22 (1981) 579–587.
- [17] H. Sakamoto, K. Shimizu, Experimental investigation on cyclic deformation and fatigue polycrystalline CuAlNi Shape memory alloys above  $M_s$ , *Trans. Jpn. Inst. Met.* 27 (1986) 592–600.
- [18] T. Baxevanis, D.C. Lagoudas, Fracture mechanics of shape memory alloys: review and perspectives, *Int. J. Fract.* 191 (2015) 191–213.
- [19] S. Miyazaki, T. Kawai, K. Otsuka, The origin of intergranular fracture in beta phase shape memory alloy, *Scr. Metall.* 16 (1982) 431–436.
- [20] C.J. Araújo, A.A.C. Gomes, J.A. Silva, A.J.T. Cavalcanti, R.P.B. Reis, C.H. Gonzalez, Fabrication of shape memory alloys using the plasma skull push/pull process, *J. Mater. Process. Technol.* 209 (2009) 3657–3664.
- [21] E.C. Pereira, PhD Thesis submitted to the State University of the Northern Rio de Janeiro, Campos dos Goytacazes, RJ, Brazil, CDD 669.96, 2009, pp. 1–224.
- [22] L.A. Matlakhova, E.C. Pereira, A.N. Matlakhov, S.N. Monteiro, in: H.R. Chen (Ed.), *Shape Memory Alloys* (Chapter 4), Nova Science Publish, 2010, pp. 113–143.
- [23] E.C. Pereira, L.A. Matlakhova, A.N. Matlakhov, S.N. Monteiro, R.J.S. Rodriguez, Effect of applied load on the characteristics of reversible martensitic transformation during thermal cycling treatment of a monocrystalline Cu-13.5Al-4Ni alloy, *Mater. Sci. Res. J.* 4 (2010) 15–36.
- [24] L.A. Matlakhova, E.C. Pereira, A.N. Matlakhov, S.N. Monteiro, R.J.S. Rodriguez, Stress assisted thermal cycling treatment of a monocrystalline Cu-Al-Ni alloy, *Mater. Sci. Res. J.* 5 (2011) 31–50.
- [25] H. Kato, K. Sasaki, Avoiding error of determining the martensite finish temperature due to thermal inertia in differential scanning calorimetry: model and experiment of Ni–Ti and Cu–Al–Ni shape memory alloys, *J. Mater. Sci.* 47 (2012) 1399–1410, <http://dx.doi.org/10.1007/s10853-011-5919-4>.
- [26] H. Warlimont, Z. Wilkens, *JCPDS* 28-0005, *Metallkd* 55 (1964) 382.
- [27] J. Karsson, *JCPDS* 07-0108, *Inst. Met.* 79 (1951) 391.
- [28] H. Friske, Z. Anorg, *JCPDS* 11-0010, *Allg. Chem.* 258 (1949) 198.
- [29] *Tech Phys Dien Delft. JCPDS* 28-0016Netherlands, ICDD, 1975.
- [30] P.H. Joneau, P. Stadelmann, <http://cecm.insa-lyon.fr/CIOLS/crystal4.pl/>, 2005 (accessed 20.06.05).
- [31] V. Recarte, J.I. Pérez-Landazábal, P.P. Rodríguez, E.H. Bocanegra, M.L. Nó, J. San Juan, Thermodynamics of thermally induced martensitic transformations in Cu–Al–Ni shape memory alloys, *Acta Mater.* 52 (2004) 3941–3948.
- [32] A. Ibarra, J. San Juan, E.H. Bocanegra, M.L. Nó, Evolution of microstructure and thermochemical properties during superelastic compression cycling in Cu–Al–Ni single crystals, *Acta Mater.* 55 (2007) 4789–4798.
- [33] A.N. Matlakhov, F.O. Braga, L.A. Matlakhova, C.J. de Araújo, Structure and Properties of alloy polycrystalline Cu–Al–Ni obtained by fusion plasma and submitted to strain compression, in: *12th Seminary of Non-ferrous Metals ABM*, 2011, pp. 78–88.
- [34] M.M. Silva, N.J. Silva, M.A. Santos, C.J. Araújo, Reprocessing Influence on Plasma in Properties of Alloy Cu–Al–Ni Shape Memory, 61<sup>st</sup> ABM Annual Congress, Rio de Janeiro, RJ, Brasil, 2006, pp. 2942–2950.
- [35] L.A. Matlakhova, E.C. Pereira, A.N. Matlakhov, S.N. Monteiro, R. Toledo, Mechanical behavior and fracture characterization of a monocrystalline Cu–Al–Ni subjected to thermal cycling treatments under load, *Mater. Charact.* 59 (2008) 1630–1637.
- [36] K. Otsuka, K. Nakai, K. Shimizu, Structure dependence of superelasticity in CuAlNi alloy, *Scr. Metall.* 8 (1974) 913–918.
- [37] Y. Nakata, T. Tadaki, K. Shimizu, Thermal cycling effects in a Cu–Al–Ni shape memory alloy, *Trans. Jpn. Inst. Met.* 26 (1985) 646–652.
- [38] E.M. Mazzer, C. Kiminami, C. Bolfarini, R.D. Cava, W.J. Botta, P. Gargarella, Thermodynamic analysis of the effect of annealing on the thermal stability of a Cu–Al–Ni–Mn shape memory alloy, *Thermochim. Acta* 608 (2015) 1–6.
- [39] M. Benke, V. Mertinger, In situ optical microscope study of the thermally induced displacive transformations in CuAlNi-based shape-memory, *J. Mater. Eng. Perform.* 23 (2014) 2333–2338.
- [40] Z. Nishiyama, *Martensitic Transformation*, Academic Press, London, UK, 1978, pp. 306–310.
- [41] R.E. Reed-Hill, R. Abbashian, *Physical Metall. Principles*, third ed., 1994, pp. 538–586.